

Multi-object investigation using two-wavelength phase-shift interferometry guided by an optical frequency comb

Dahi Ghareab Abdelsalam Ibrahim^{1,2,3,a)} and Takeshi Yasui^{2,3}

¹Engineering and Surface Metrology Lab., National Institute of Standards, Tersa St., El haram, El Giza, Egypt

²Graduate School of Technology, Industrial and Social Sciences, Tokushima University, 2-1, Minami-Josanjima, Tokushima 770-8506, Japan

³JST, ERATO, MINOSHIMA Intelligent Optical Synthesizer Project, 2-1, Minami-Josanjima, Tokushima 770-8506, Japan

(Received 30 January 2018; accepted 3 April 2018; published online 23 April 2018)

Two-wavelength phase-shift interferometry guided by optical frequency combs is presented. We demonstrate the operation of the setup with a large step sample simultaneously with a resolution test target with a negative pattern. The technique can investigate multi-objects simultaneously with high precision. Using this technique, several important applications in metrology that require high speed and precision are demonstrated. *Published by AIP Publishing.*

<https://doi.org/10.1063/1.5024244>

Phase shift interferometry (PSI) is an optical metrology technique used for surface micro-topography measurements with excellent accuracy.¹⁻⁴ However, the phase distribution suffers from 2π discontinuities, which set a limit to the phase measurement range of single-wavelength. Two-wavelength PSI provides a solution to this ambiguous phase problem with the use of a beat wavelength λ_{beat} from two wavelengths λ_1 and λ_2 . As a result, the phase measurement range is extended to a longer λ_{beat} . However, it involves a shortcoming of being susceptible to instability of the two wavelengths used. Instability of the two-wavelengths used might introduce a fluctuation in the beat wavelength, and hence an inherent phase error arises. We expect that this error is maximized when longer λ_{beat} is used to examine surfaces with large steps. Also, such wavelength instability limits the minimum difference between two wavelengths, and hence the maximum λ_{beat} .

An interesting wavelength reference to suppress the wavelength instability is an optical frequency comb (OFC).^{5,6} The OFC is composed of a series of frequency spikes regularly spaced by a repetition frequency f_{rep} with a carrier-envelope-offset frequency f_{ceo} and can be used as an optical frequency ruler traceable to a frequency standard by its mode-locking nature and laser stabilization. If a tunable narrow-linewidth continuous-wave (CW) laser, e.g., an external cavity laser diode (ECLD), is phase-locked to one mode of OFC, the inherent characteristics of OFC (narrow linewidth, high stability, high accuracy, etc.) are transferred to the CW laser. Furthermore, the CW laser can be tuned at a step of f_{rep} by changing the phase-locked OFC mode. The phase-locked CW laser, namely the optical frequency synthesizer (OFS)⁷ is traceable to the frequency standard via OFC, and hence largely suppresses the wavelength instability.

In this letter, we minimized the inherent phase error and expanded the beat wavelength by introducing an OFS into two-wavelength PSI. This technique makes it possible to feature large stepped structures as large as meter depth with

nanometer resolution. We use this merit to investigate two objects in real-time (multi-objects simultaneously) with high precision. This technique can be applied to test a burst of identical objects in real time for onsite production lines.

We here used a Mach-Zehnder interferometer to produce the interference pattern. The intensity of the interference signal is given as follows:⁸

$$I_j = a + b \cos(\phi + (j-1)\pi/2), \quad (1)$$

where a is the so-called DC level, b is the modulation, $j=1-4$ in the case of four frames, and ϕ is the phase of the interference signal. The interference phase is related to the optical path difference (Δz) between the two beams of the interferometer as follows:

$$\phi(\lambda_i) = (2\pi/\lambda_i)\Delta z, \quad (2)$$

where λ is the wavelength of the illuminating light source and $i=1-2$. The phase information encoded in the fringe structure of the interferogram is recovered by the PSI technique via changing the reference arm length of the interferometer in four equal steps with a step size equivalent to the $\pi/2$ phase shift;⁹ for each step, the interference signal is recorded. Using these four phase-shifted signals of Eq. (1), the phase is extracted for each point of the objects as

$$\phi = \tan^{-1}[(I_4 - I_2)/(I_1 - I_3)]. \quad (3)$$

A phase unwrapping algorithm to unwrap the 2π module of the wrapped phase is applied because step heights of the objects being tested are greater than one fringe of the interference signal.^{1,10} Here, we used signals of two wavelengths λ_1 and λ_2 . For each wavelength, four phase-shifted signals are captured successively, and the single-wavelength phase is computed by applying Eq. (3). Then, by subtracting the phase image $\phi(\lambda_1)$ of λ_1 from the phase image $\phi(\lambda_2)$ of λ_2 , a beat phase image ϕ_{beat} can be written as

$$\phi_{beat} = \phi(\lambda_2) - \phi(\lambda_1), \quad (4)$$

^{a)}Author to whom correspondence should be addressed: dahi.abdelsalam@nis.sci.eg

where the beat phase image is synthesized that allows for imaging much larger axial ranges. The beat wavelength can be formulated using

$$\lambda_{beat} = \lambda_1 \lambda_2 / (\lambda_1 - \lambda_2). \quad (5)$$

By measuring the beat wavelength and the synthesized phase, the height can be calculated precisely as

$$h = (\phi_{beat}/4\pi)\lambda_{beat}. \quad (6)$$

From Eq. (6), it is evident that any small variation in the beat wavelength produces an error in the reconstructed height; so, it is essential to stabilize the wavelengths employed to investigate the objects. The present OFS was achieved by phase-locking a tunable ECLD to one mode of the OFC. Figure 1 shows a description of an ECLD and an OFC in the optical frequency domain. The optical frequency ν_{CW} of the OFS is given by¹¹

$$\nu_{CW} = f_{ceo} + n f_{rep} + f_{beat}, \quad (7)$$

where n is the mode number of the OFC (typically, $\sim 10^6$) phased-locked by an ECLD, and f_{beat} is the beat frequency between the ECLD and the n -th OFC mode. ν_{CW} can be tuned at a step of f_{rep} by changing the n value, while maintaining the phase-locking to the frequency standard. An upper part of Fig. 2 shows an experimental setup of OFS, which is composed of a tunable ECLD (LT-5001N, OptoComb, Inc., optical wavelength range = 188.5 THz–197.2 THz, wavelength range = 1520 nm–1590 nm, mean power = 30 mW) and a commercialized fiber OFC laser (FC1500–250-WG, Menlo Systems GmbH, Munich, Germany, center wavelength = 1550 nm, spectral bandwidth = 73 nm, and mean power = 380 mW). f_{ceo} and f_{rep} were, respectively, set to 20 MHz and 250 MHz by phase-locking to a rubidium (Rb) atomic clock (FS725, Stanford Research Systems, accuracy = 5×10^{-11} and instability = 2×10^{-11} at 1 s) using accompanying stabilization electronics. Output lights from the ECLD and the OFC were spatially overlapped by a polarization beam splitter (PBS) and half-wave plates ($\lambda/2$) together with power adjustment. After passing through another $\lambda/2$, a polarizer, and a diffraction grating, the f_{beat} signal was detected by a photodiode (PD). f_{beat} was set to 30 MHz by phase-locking to the same frequency standard using a proportional-integral-derivative (PID) controller. The n value can be determined by a wavelength meter (AQ6151, Yokogawa Test & Measurement Corp., wavelength accuracy = 0.3 pm). Finally, ν_{CW} can be tuned at a step of 250 MHz ($=f_{rep}$) within the range of 188.5 THz to 197.2 THz. The corresponding wavelength λ_{CW} can be tuned at a step of 2 pm within the range of 1520 nm to 1590 nm. The optical frequencies ν_{CW1}

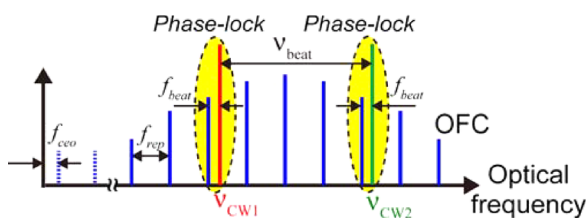


FIG. 1. Description of the ECLD and the OFC in the optical frequency domain.

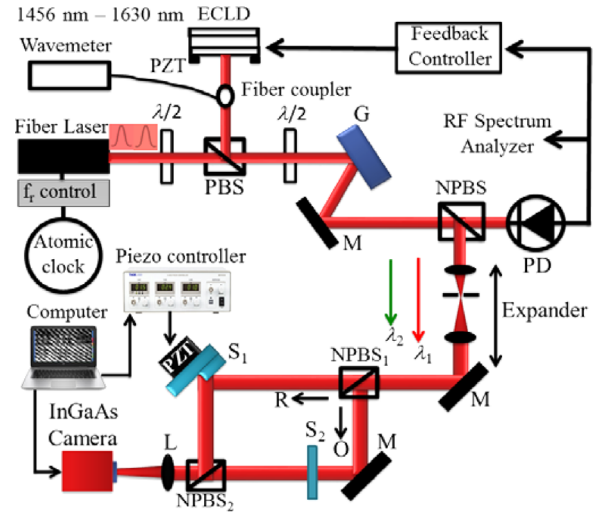


FIG. 2. Experimental setup. ECLD, external cavity laser diode; PZT, piezoelectric transducer; G, grating; M, mirror; PBS, polarizing beam splitter; NPBS, non-polarizing beam splitter; PD, photodetector; S_1 , first object of step height of around 7.201 mm (employed also as a reference); and S_2 , second object of a USAF resolution target with a negative pattern.

and ν_{CW2} of the OFS were adjusted in series by changing n . The optical beat frequency ν_{beat} between them is related to the beat wavelength λ_{beat} by

$$\nu_{beat} = \nu_{CW2} - \nu_{CW1} = c \frac{\lambda_{CW1} - \lambda_{CW2}}{\lambda_{CW1} \lambda_{CW2}} = \frac{c}{\lambda_{beat}}, \quad (8)$$

where c is the speed of light and λ_{CW1} and λ_{CW2} are wavelengths corresponding to ν_{CW1} and ν_{CW2} . The present OFS has the ability to generate two-wavelength light with an arbitrary wavelength difference ($2 \text{ pm} < \lambda_1 - \lambda_2 < 70 \text{ nm}$), corresponding to the beat wavelength from $35 \mu\text{m}$ to 1.2 m.

An experimental setup of two-wavelength PSI is shown in the lower part of Fig. 2. Output light from the OFS was fed into the Mach-Zehnder interferometer. After recombining both beams, the off-axis holograms were captured at two different wavelengths by a cooled InGaAs CCD camera (Goldeye P-008, Allied Vision Technol. GmbH, 320×256 pixels, pixel size = $30.0 \mu\text{m}$), and then reconstructed with a four-step PSI algorithm.³ The variations in the optical path length of one arm were done by a piezoelectric transducer (PZT).

A reflection object S_1 and a transmission object S_2 were used as samples. S_1 is a step height of around 7.201 mm (measured roughly by a digital micrometer) positioned at reflection in the reference arm of the interferometer, while S_2 is a USAF (United States Armed Forces) resolution test target with a negative pattern positioned at transmission in the object arm of the interferometer. In order to image the two objects S_1 and S_2 in the imaging plane of the camera, the second object S_2 was placed in a suitable distance in the object arm related to the power of the imaging lens L (NA = 0.4). A schematic drawing of S_1 is shown in Fig. 3(a). Photographs of both S_1 and S_2 taken with the proposed setup with blocking of the two arms of the interferometer mutually are shown in Figs. 3(b) and 3(c), respectively. The two objects were investigated simultaneously by using two different wavelengths at $\lambda_1 = 1540.403 \text{ nm}$ and $\lambda_2 = 1541.403 \text{ nm}$.

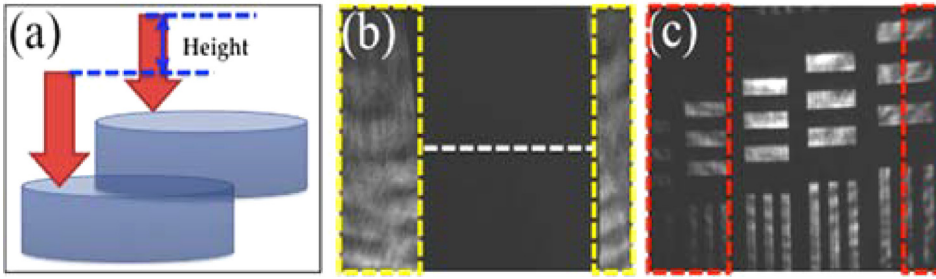


FIG. 3. (a) Representation of the reflected type object, (b) a photograph of 12 mm of (a), and (c) a photograph of the transmissive USAF object.

Once S_1 and the gold mirror (in the absence of S_2) constitute the off-axis interferogram, S_2 is introduced in the other arm. The obtained off-axis hologram is deformed in accordance with the patterns of S_2 . For each wavelength, four phase-shifted off-axis interferograms were recorded successively. The change in the optical pathlength was done by actuating S_1 using a closed-loop PZT with a linearity of up to 0.15%. Figures 4 and 5 show four phase-shifted images at two different wavelengths $\lambda_1 = 1540.403$ nm and $\lambda_2 = 1541.403$ nm, respectively. For each wavelength, the 3D phase map is computed in accordance with Eq. (3). As seen in Figs. 4 and 5, the off-axis fringes appear clearly inside the yellow and red rectangles of both objects shown in Figs. 3(b) and 3(c).

Since the arctan function produces values only in the range of $[-\pi/2, \pi/2]$, as shown in Fig. 6, the wrapped phase for each wavelength is unwrapped^{9,10} to remove the ambiguity in the phase. Figures 7(a) and 7(b) show the unwrapped phases of Figs. 6(a) and 6(b), respectively. By subtracting the phases of Figs. 7(a) and 7(b), an equivalent phase image is synthesized, as shown in Fig. 7(c).

As seen in Fig. 7(c), all the illuminated patterns of S_1 and S_2 are extracted into a single image. Based on the synthesized phase image of Fig. 7(c) and the beat wavelength, the step-height of S_1 as well as the heights of the patterns in S_2 are precisely obtained using Eq. (6). The phase profile extracted horizontally along the red line (S_1) in the synthesized phase of Fig. 7(c) is shown in Fig. 7(d), indicating the cross-sectional profile of 320 pixels. Here, the X-axis is reversed to see the phases from different angles of view.¹² Based on Fig. 7(d), the $\phi_{beat} = 38$ rad (the difference between the blue lines). The beat wavelength is calculated

using Eq. (5) to be $\lambda_{beat} = 2.3744e^{+6}$ nm. By substituting the values of ϕ_{beat} and λ_{beat} in Eq. (6), the step height is estimated to be 7.180 mm [no image enhancement technique was applied to Fig. 7(d)], which is in excellent agreement with the nominal value.

The heights of the patterns of S_2 can also be extracted from the same synthesized phase image of Fig. 7(c). The phase profiles extracted vertically along both blue and black lines of Fig. 7(c) were corrected from noise by applying the high pass filter,¹³ and the corrected phase profiles are shown in Figs. 8(a) and 8(b), respectively. The benefit of this filter is to mitigate the coherent noise to some amount. The beat phase along the blue and black lines of Fig. 7(c) before correction with a high pass filter was estimated to be ($\phi_{beat} = 5.9$ rad), while after correction, it is estimated to be ($\phi_{beat} = 3.2$ rad) as shown in Fig. 8. By substituting the values of ϕ_{beat} and λ_{beat} in Eq. (6), the step height is estimated to be 0.605 mm.

We claim that image enhancement techniques such as flat fielding with apodization may improve the edges in Fig. 8,^{14–16} and this will be the next step of our future research. Here, the measurement precision of the object surface depends on the wavelength stability and the robustness of the interferometer to surrounding external disturbances such as air turbulence or vibration. Although the optical comb largely enhances the stability of the frequency and the phase of two-wavelength light, surrounding external disturbances essentially limits the phase noise to $\lambda/100 - \lambda/1000$. For that reason, we expect that using single-shot parallel four-step PSI will minimize the error in measurement, and this will also be the next step of our future research.

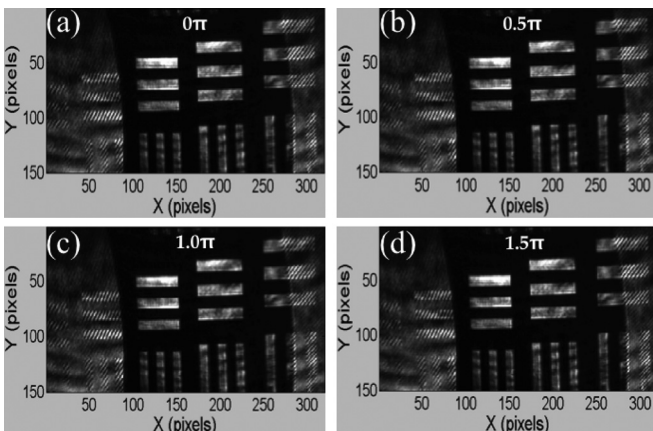


FIG. 4. Four phase-shifted images of one wavelength $\lambda_1 = 1540.403$ nm captured by a cooled In-GaAs camera.

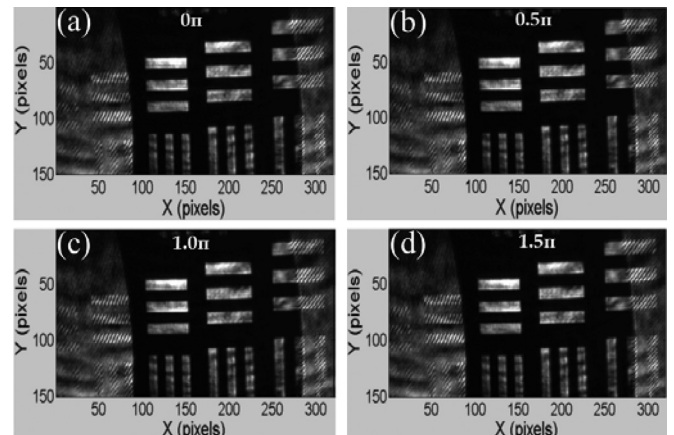


FIG. 5. Four phase-shifted images of one wavelength $\lambda_1 = 1541.403$ nm captured by a cooled In-GaAs camera.

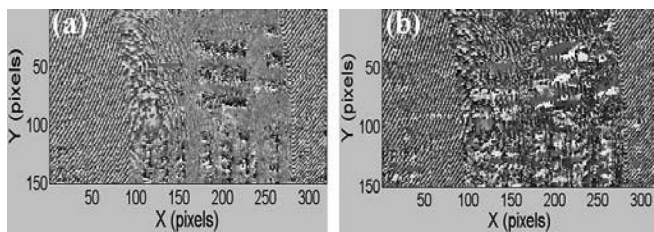


FIG. 6. (a) Wrapped phase map of Fig. 4 and (b) wrapped phase map of Fig. 5.

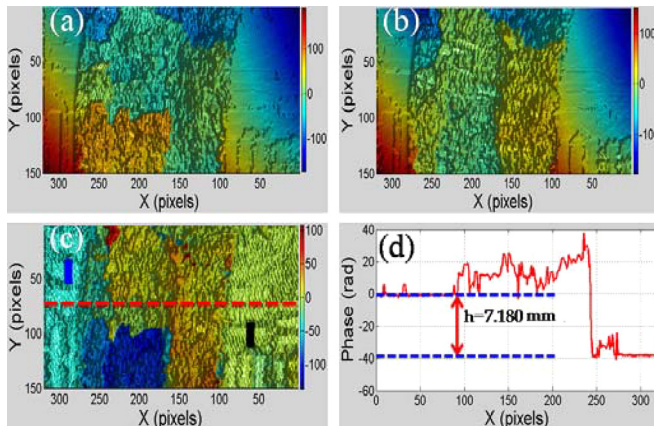


FIG. 7. (a) Unwrapped phase map of Figs. 6(a) and (b) the unwrapped phase map of Fig. 6(b). (c) Difference between (a) and (b). (d) 1D phase profile along the red line of (c).

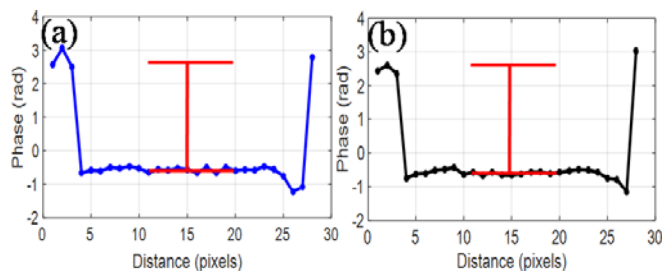


FIG. 8. (a) 1D phase profile along the blue line of Fig. 7(c) and (b) a 1D phase profile along the black line of Fig. 7(c). The profiles shown here are after application of the high pass filter process.

In conclusion, we have presented an optical metrology technique for measuring the 3D surface profiles of many objects simultaneously with high precision. Excellent results were extracted with all featured patterns in a single shot. The term high precision here refers to the highly stable wavelengths

secured by the frequency standard via the OFC. The technique is fully operable for samples having large step heights as large as meter depth with nanometer resolution. Merit of this technique is that it can be used onsite in a production line to test identical objects in real time. The mechanism can be done as follows: a calibrated object is positioned at reflection in the reference arm of the interferometer and a burst of same objects being tested are positioned in the object arm in the interferometer. From the difference in the phase between the calibrated object and the object being tested, the performance of the object being tested is assigned. If the difference in the phase equals zero, this means a perfect tested object, if not, means a re-conditioning is needed. Future improvement of the system includes use of this technique with a single-shot parallel four-step, dual-wavelength PSI interferometry, which is expected to increase the SNR and improve the accuracy of measurement.

Funding was provided by Exploratory Research for Advanced Technology (ERATO), Japanese Science and Technology Agency (MINOSHIMA Intelligent Optical Synthesizer Project, JPMJER1304) and Mitutoyo Association for Science and Technology.

¹Y. Y. Cheng and J. C. Wyant, *Appl. Opt.* **23**, 4539–4543 (1984).

²M. Born and E. Wolf, *Principles of Optics* (Cambridge University Press, Cambridge, England, 1980).

³D. G. Abdelsalam and D. Kim, *Appl. Opt.* **50**, 6153 (2011).

⁴X. He, D. Zou, S. Liu, and Y. Guo, *Opt. Eng.* **37**, 1419 (1998).

⁵T. Udem, R. Holzwarth, and T. W. Hänsch, “Optical frequency metrology,” *Nature* **416**, 233–237 (2002).

⁶N. Schuhler, Y. Salvadé, S. Lévêque, R. Dändliker, and R. Holzwarth, “Frequency-comb-referenced two-wavelength source for absolute distance measurement,” *Opt. Lett.* **31**(21), 3101–3103 (2006).

⁷H. Takahashi, Y. Nakajima, H. Inaba, and K. Minoshima, “Ultra-broad absolute-frequency tunable light source locked to a fiber-based frequency comb,” in *Lasers and Electro Optics, 2009 and Conference on Quantum Electronics and Laser Science, CLEO/QELS (2009)*, p. CTuK4.

⁸E. Wolf, *Progress in Optics* (Elsevier, 1988), pp. 351–366.

⁹M. Takeda, H. Ina, and S. Kobayashi, *J. Opt. Soc. Am.* **72**, 156 (1982).

¹⁰H. van Brug, *Appl. Opt.* **37**, 6701–6706 (1998).

¹¹J. Ye and S. T. Cundiff, *Femtosecond Optical Frequency Comb: Principle, Operation and Applications* (Springer science + Business Media, USA, 2005).

¹²D. G. Abdelsalam and T. Yasui, *Appl. Opt.* **56**, F1–F6 (2017).

¹³F. Ahmed and M. S. Mohamud, *Int. J. Sci. Res. Publ.* **5**, 1–6 (2015).

¹⁴D. G. Abdelsalam and D. Kim, *Opt. Express* **19**, 17951 (2011).

¹⁵D. G. Abdelsalam, M. S. Shaalan, and M. M. Eloker, *Opt. Lasers Eng.* **48**, 543 (2010).

¹⁶D. G. Abdelsalam, M. S. Shaalan, M. M. Eloker, and D. Kim, *Opt. Lasers Eng.* **48**, 643 (2010).